1

Introduction to Synthesized Transmission Lines

C. W. Wang and T. G. Ma

1.1 Introduction

In modern communication systems, the rapid evolution of integrated circuit (IC) and packaging technologies have driven more and more function blocks to be integrated into a single chip/module. In the second decade of the twenty-first century, highly-integrated front-end modules such as microwave/millimeter-wave radar and image systems, [1–4], phased arrays [5, 6], and so on have hit the commercial markets. In general, the RF modules require a large number of transmission-line-based elements for vector signal processing in the analog domain. The transmission line elements, however, inevitably occupy a large circuit area. In the cost-driven market, area is the cost. It therefore leads to an enormous amount of research work focusing on developing various kinds of synthesized transmission lines for reducing the required circuit size. A synthesized transmission line is a lumped or quasi-lumped network that may function identically to a uniform transmission line within a given bandwidth.

Synthesized transmission lines can be developed with or without periodicity. In a broad sense, it could be either right-handed or left-handed depending on the forming blocks. To describe the general concept, in this chapter we will start from Maxwell's equations and discuss the analog between plane wave propagation in a material media and the TEM mode in a parallel-plate waveguide. The parameters associated with the wave propagation and their corresponding circuit parameters in a transmission line are linked herein. Based on the fundamental principle, design formulae for periodic and non-periodic synthesized transmission lines are summarized. Classical design approaches are reviewed to demonstrate how synthesized transmission lines are realized practically. A brief review of left-handed synthesized lines, or metamaterial structures, is provided at the end of the chapter.

Synthesized Transmission Lines: Design, Circuit Implementation, and Phased Array Applications, First Edition.
Tzyh-Ghuang Ma, Chao-Wei Wang, Chi-Hui Lai and Ying-Cheng Tseng.

The formulae in this chapter form the basis of the non-periodic synthesized transmission lines in Chapter 2 for circuit miniaturization, and in Chapter 5 for chip implementation. The multi-operational mode synthesized transmission lines in Chapters 3 and 4, for phased array applications, are also derived using the same building blocks. The two-dimensional synthesized transmission lines in Chapter 6 also follow the periodic condition in Sec. 1.3.1.

1.2 Propagation Characteristics of a TEM Transmission Line

In this section, we start with the Maxwell's equations to derive the governed equations in a wave-guiding structure under the assumption of a transverse electromagnetic (TEM) field distribution. The propagation characteristics are summarized and compared to a distributed transmission line having similar mathematical forms by using circuit parameters.

1.2.1 Wave Equations

As shown in Fig. 1.1, consider a parallel-plate waveguide operated in the TEM mode. The field distribution inside the wave-guiding structure is known to be identical to a uniform plane wave in free space with uniquely defined voltage and current in the transverse plane. Maxwell's curl equations in a source-free region are:

$$\nabla \times \vec{E} = -\mu \frac{\partial \vec{H}}{\partial t}, \tag{1.1}$$

$$\nabla \times \vec{H} = \varepsilon \frac{\partial \vec{E}}{\partial t}. \tag{1.2}$$

Assuming that the wave propagates along the z-direction, the fields transverse to the direction of propagation in a parallel-plate waveguide, from (1.1) and (1.2), are:

$$\frac{-\partial E_x}{\partial z} = \mu \frac{\partial H_y}{\partial t}, \tag{1.3}$$

$$\frac{-\partial H_y}{\partial z} = \varepsilon \frac{\partial E_x}{\partial t}. \tag{1.4}$$

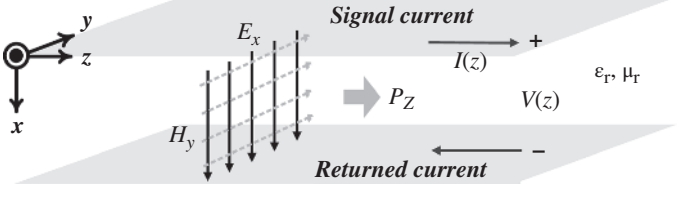

Figure 1.1 Wave propagation in a parallel-plate waveguide

Partially differentiate (1.3) with respect to z and (1.4) with respect to t to get,

$$\frac{-\partial^2 E_x}{\partial z^2} = \mu \frac{\partial^2 H_y}{\partial z \partial t}, \tag{1.5}$$

$$\frac{-\partial^2 H_y}{\partial t \partial z} = \varepsilon \frac{\partial^2 E_x}{\partial t^2}, \tag{1.6}$$

Substitution of (1.6) into (1.5) yields

$$\frac{\partial^2 E_x}{\partial^2 z} = \mu\varepsilon \frac{\partial^2 E_x}{\partial^2 t}. \tag{1.7}$$

It is a second-order partial differential equation known as the *one-dimensional wave equation*, which can be applied to any wave-guiding structure supporting TEM wave propagation. The phase velocity of the TEM wave is simply

$$v_p = \frac{1}{\sqrt{\mu\varepsilon}}. \tag{1.8}$$

where μ and ε are the permeability and permittivity of the medium filled within the wave-guiding structure.

Now, let us turn our attention to a lossless distributed uniform transmission line modeled by periodically loaded *LC* sections, as shown in Fig. 1.2. Under the assumption that each lumped *LC* segment is infinitesimal in length, the voltage and current along the line, from Kirchhoff's laws, are related to each other by,

$$\frac{-\partial V}{\partial z} = L \frac{\partial I}{\partial t}, \tag{1.9}$$

$$\frac{-\partial I}{\partial z} = C \frac{\partial V}{\partial t}. \tag{1.10}$$

L and C are the per-unit-length inductance and capacitance of the line. Equations (1.9) and (1.10) are known as the *Telegrapher's equations* and actually take the same form as (1.3) and (1.4).

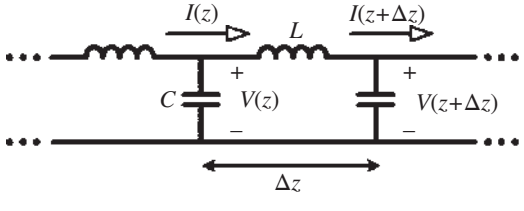

Figure 1.2 Equivalent lumped *LC* model of a distributed uniform transmission line

Following the same mathematical procedure, the wave equation is derived in terms of the voltage (V) or current (I) as,

$$\frac{\partial^2 V}{\partial^2 z} = LC\frac{\partial^2 V}{\partial^2 t}. \tag{1.11}$$

The general solution of the voltage and current waves propagated along the lossless uniform transmission line, from (1.11), is

$$V(z) = V^+ e^{-j\beta z} + V^- e^{+j\beta z}, \tag{1.12}$$

$$I(z) = I^+ e^{-j\beta z} - I^- e^{+j\beta z}. \tag{1.13}$$

β is known as the *phase constant* or *guided wavenumber*,

$$\beta = \frac{\omega}{v_p} = \omega\sqrt{LC}. \tag{1.14}$$

The phase velocity of the voltage and current waves is therefore,

$$v_p = \frac{1}{\sqrt{LC}}. \tag{1.15}$$

Meanwhile, differentiating (1.12) with respect to z, we have

$$\frac{\partial V(z)}{\partial z} = -j\beta V^+ e^{-j\beta z} + j\beta V^- e^{+j\beta z} = -j\omega L I(z). \tag{1.16}$$

Substitution of (1.13) into (1.16) yields

$$-j\beta V^+ e^{-j\beta z} + j\beta V^- e^{+j\beta z} = -j\omega L I^+ e^{-j\beta z} + j\omega L I^- e^{+j\beta z}. \tag{1.17}$$

From (1.17), the *characteristic impedance* of a lossless transmission line is then defined as,

$$Z_c = \frac{V^+}{I^+} = \frac{V^-}{I^-} = \frac{\omega L}{\beta} = \sqrt{\frac{L}{C}} = v_p L = \frac{1}{v_p C}. \tag{1.18}$$

It is interesting to note that (1.3)–(1.8), (1.9)–(1.13), and (1.15) are actually in the same form, suggesting that under the TEM-mode operation, the electromegnetic (EM) parameters of a wave-guiding structure can be mapped one-to-one onto the circuit parameters of its transmission-line equivalence. The wave impedance of the parallel-plate waveguide in Fig. 1.1 is in the same form as the characteristic impedance in (1.18), as well.

Table 1.1 Analog between EM parameters in a TEM parallel-plate waveguide and circuit parameters in a uniform transmission line

EM Parameters	Circuit Parameters
E: Electric field intensity (V/m)	V: Voltage wave (V)
H: Magnetic field intensity (A/m)	I: Current wave (A)
ε: Permittivity (F/m)	C: Capacitance per meter (F/m)
μ: Permeability (H/m)	L: Inductance per meter (H/m)

Table 1.1 summarizes the analog between the EM parameters of a TEM wave-guiding structure and the circuit parameters of a lossless transmission line. The mapping holds exactly for TEM transmission lines and approximately for quasi-TEM ones. To simplify the design procedure, hereafter we will use the scalar circuit parameters (V, I, L, C) to analyze the propagation characteristics of any kind of TEM/quasi-TEM transmission lines.

1.2.2 Keys to Miniaturization

In Sec. 1.2.1, the wave equation and general solution of a TEM transmission line are derived in terms of the field parameters (E, H, μ, ε) as well as circuit parameters (V, I, L, C) at the same time. In this section, we further introduce the slow wave factor as a figure of merit for judging the circuit miniaturization capability of a given wave-guiding structure.

First of all, recall the guided wavenumber can be expressed in terms of both EM and circuit parameters as

$$\beta_g = \frac{\omega}{v_p} = \omega\sqrt{LC} = \omega\sqrt{\mu\varepsilon} = \omega\sqrt{\mu_r\mu_o\varepsilon_r\varepsilon_o}. \tag{1.19}$$

The free space wavenumber, or the phase constant of a wave propagated in free space, is

$$\beta_o = \omega\sqrt{\mu_o\varepsilon_o}. \tag{1.20}$$

The *slow wave factor* is defined as the ratio of the guided wavenumber to free space wavenumber as

$$SWF = \frac{\beta_g}{\beta_o} = \frac{\lambda_o}{\lambda_g} = \sqrt{\mu_r\varepsilon_r} = c\sqrt{LC}. \tag{1.21}$$

c is the speed of light in vacuum. The slow wave factor is a measure of how good a wave-guiding structure can be used for circuit miniaturization.

Meanwhile, a section of transmission line is commonly expressed in terms of its *electrical length* at the operating frequency as

$$\theta = \beta_g l. \tag{1.22}$$

l is the physical length of the line section. From (1.22), for a given electrical length, increasing the guided wavenumber (β_g) becomes the key factor to reduce the required physical length of a transmission line. Choosing a material media with a higher ε_r or μ_r is a possible way to reduce the physical length with a larger β_g. However, it is likely at the expense of higher fabrication cost. Alternatively, using synthesized transmission lines in accordance with (1.19) and (1.22) paves another way for circuit miniaturization by simultaneously increasing the per-unit-length inductance and capacitance of that line. Here, the *synthesized transmission line* is referred to as any microwave lumped/quasi-lumped network that can be electrically equivalent to a section of uniform transmission line over a frequency band of interest.

A further thought on developing a synthesized transmission line is: in a practical circuit, how can we fulfill the goal by simultaneously increasing the inductance and capacitance of a line? The answer is quite straightforward: "*just follow the fundamental physical rules*." An extra current path always generates additional magnetic fields and, hence, the inductance. The charge accumulation between electrodes, in the meantime, results in extra capacitive loadings. Accordingly, using a meander or spiral high-impedance line is an effective way to provide more current paths or higher current density to increase the per-unit-length inductance in a real design. Meanwhile, adding parallel-plate or interdigital capacitor is a good way to boost the capacitance of the host transmission line. When one attempts to adjust the per-unit-length inductance and capacitance for raising the slow wave factor, it is interesting to note that the characteristic impedance of the line can be controlled at the same time using (1.18) within a reasonable range, say, 20–120 Ω.

Quite a few synthesized transmission lines (or the so-call artificial transmission lines) are summarized and listed in [7]. Some of them are redrawn in Fig. 1.3 for easy reference [8–16]. They are all designed based on alternatively connected series inductance and shunt capacitance with or without periodicity. This sort of synthesized lines is right-handed in nature with lowpass responses. Readers are encouraged to find clues on how the line inductance and capacitance in the examples are boosted. Following the same rule, the readers can develop new and creative structures on their own. In fact, the number of layout patterns of a synthesized transmission line with given electrical properties can be extended to infinity!

Finally, although the aforementioned discussion is restricted to lossless transmission lines, similar statements hold true for a low-loss one. The only difference is the introduction of the

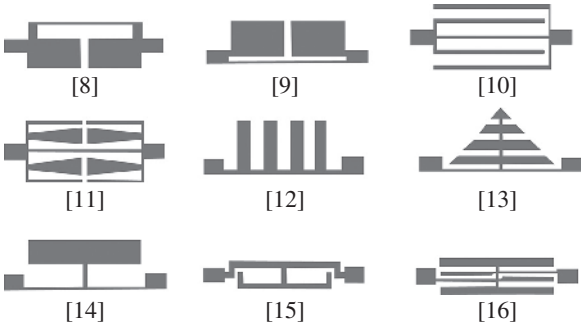

Figure 1.3 Typical slow-wave synthesized transmission lines in open literature

attenuation constant (α), which results in a *complex propagation constant* ($\gamma=\alpha+j\beta$) with a small real part representing the loss. The quality factor (Q) is evaluated by

$$Q=\frac{\beta}{2\alpha}. \tag{1.23}$$

In the following section, the common ways to analyze a periodic or non-periodic synthesized transmission line are introduced as the basis of the entire book.

1.3 Analysis of Synthesized Transmission Lines

Synthesized transmission lines can be realized with or without periodicity. While the non-periodic lines can be dealt with using simple transmission line equivalence, the periodic lines are in general analyzed by the *Bloch theorem* [17]. In this section, the general analysis procedures for periodic and non-periodic synthesized transmission lines are introduced in sequence as follows.

1.3.1 Bloch Theorem and Characterization of a Periodic Synthesized Transmission Line

Figure 1.4 shows a typical periodically-loaded synthesized transmission line. It comprises a uniform transmission line of (Z_c) (*the host line*) periodically loaded by lumped or quasi-lumped shunt elements (*jb*). The line is composed of infinite elements in cascade, with each element termed as a *unit cell*. The voltage and current waves on the *nth* and $(n+1)$*th* nodes are related by the *ABCD* matrix of the unit cell as

$$\begin{bmatrix} V_n \\ I_n \end{bmatrix}=\begin{bmatrix} A & B \\ C & D \end{bmatrix}\begin{bmatrix} V_{n+1} \\ I_{n+1} \end{bmatrix}. \tag{1.24}$$

Let the unit cell have a periodicity of p and the complex propagation constant equal to γ, we have

$$\begin{cases} V_{n+1}=V_n\cdot e^{-\gamma p} \\ I_{n+1}=I_n\cdot e^{-\gamma p} \end{cases}. \tag{1.25}$$

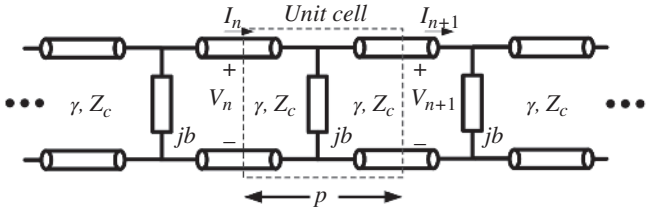

Figure 1.4 Typical periodically-loaded synthesized transmission line

Substitution of (1.25) into (1.24) yields

$$\begin{bmatrix} V_n \\ I_n \end{bmatrix} = \begin{bmatrix} A & B \\ C & D \end{bmatrix} \begin{bmatrix} V_{n+1} \\ I_{n+1} \end{bmatrix} = \begin{bmatrix} V_{n+1} \cdot e^{\gamma p} \\ I_{n+1} \cdot e^{\gamma p} \end{bmatrix}. \tag{1.26}$$

or

$$\begin{bmatrix} A - e^{\gamma p} & B \\ C & D - e^{\gamma p} \end{bmatrix} \begin{bmatrix} V_{n+1} \\ I_{n+1} \end{bmatrix} = 0. \tag{1.27}$$

For a nontrivial solution of (V_{n+1}, I_{n+1}), the determinant of the matrix must be zero, which leads to

$$AD + e^{2\gamma p} - \left(A + D\right)e^{\gamma p} - BC = 0. \tag{1.28}$$

Since the unit cell is a reciprocal network, we have $AD - BC = 1$. Thus,

$$e^{2\gamma p} - \left(A + D\right)e^{\gamma p} + 1 = 0. \tag{1.29}$$

From (1.29), the propagation constant can be expressed in terms of the *ABCD* matrix as

$$\cosh\left(\gamma p\right) = \frac{A + D}{2}. \tag{1.30}$$

In lossless case with $\alpha = 0$, (1.30) is reduced to

$$\cos\left(\beta p\right) = \frac{A + D}{2}. \tag{1.31}$$

In a periodic synthesized transmission line, the phase constant of the line can be solved from the *ABCD* matrix of the unit cell with a given periodicity p (i.e., physical length) in accordance with (1.31). In the meantime, the characteristic impedance of the unit cell can be defined as

$$Z_B = \frac{V_{n+1}}{I_{n+1}}. \tag{1.32}$$

This impedance is also called the *Bloch impedance*. From (1.27), we have

$$\left(A - e^{\gamma p}\right)V_{n+1} + BI_{n+1} = 0. \tag{1.33}$$

Substitution of (1.33) into (1.32), the Bloch impedance is

$$Z_B = \frac{-B}{A - e^{\gamma p}}. \tag{1.34}$$

From (1.29), $e^{\gamma p}$ can be solved as

$$e^{\gamma p} = \frac{(A+D) \pm \sqrt{(A+D)^2 - 4}}{2}. \tag{1.35}$$

The Bloch impedance in terms of the *ABCD* matrix is therefore

$$Z_B^{\pm} = \frac{-2B}{A - D \mp \sqrt{(A+D)^2 - 4}}. \tag{1.36}$$

If the unit cell is a symmetric network such as the case in Fig. 1.4, we have $A = D$ and the Bloch impedance can be simplified as

$$Z_B^{\pm} = \frac{\pm B}{\sqrt{A^2 - 1}}. \tag{1.37}$$

Equations (1.31) and (1.37) are the synthesis basis of all sort of one-dimensional periodic structures. They will be used intensively in Chapter 6 for analyzing a periodic synthesized transmission line with two-dimensional routing capability.

1.3.2 Characterization of a Non-Periodic Synthesized Transmission Line

The characterization of a non-periodic synthesized transmission line starts from equating the *ABCD* matrix of the network under development to that of a uniform transmission line with a given characteristic impedance and electrical length, say, Z_c and θ. The equivalences are illustrated in Fig. 1.5. Here, three-element networks, i.e. π-/T-models, are analyzed as an illustration.

The *ABCD* matrices of the π-/T-models are:

$$\begin{bmatrix} A & B \\ C & D \end{bmatrix}_{STL,\pi} = \begin{bmatrix} 1 & 0 \\ Y & 1 \end{bmatrix} \begin{bmatrix} 1 & Z \\ 0 & 1 \end{bmatrix} \begin{bmatrix} 1 & 0 \\ Y & 1 \end{bmatrix} = \begin{bmatrix} 1+ZY & Z \\ Y(2+ZY) & 1+ZY \end{bmatrix}, \tag{1.38a}$$

$$\begin{bmatrix} A & B \\ C & D \end{bmatrix}_{STL,T} = \begin{bmatrix} 1 & Z \\ 0 & 1 \end{bmatrix} \begin{bmatrix} 1 & 0 \\ Y & 1 \end{bmatrix} \begin{bmatrix} 1 & Z \\ 0 & 1 \end{bmatrix} = \begin{bmatrix} 1+ZY & Z(2+ZY) \\ Y & 1+ZY \end{bmatrix}. \tag{1.38b}$$

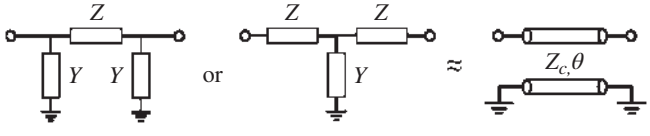

Figure 1.5 Three-element networks as non-periodic synthesized lines and their transmission line equivalence

The *ABCD* matrix of a uniform transmission line is given by

$$\begin{bmatrix} A & B \\ C & D \end{bmatrix}_{TLine} = \begin{bmatrix} \cos\theta & jZ_c \sin\theta \\ jY_c \sin\theta & \cos\theta \end{bmatrix}. \tag{1.39}$$

By equating the corresponding entries in both matrices, one gets;

$$Z_{STL,\pi} = \sqrt{\frac{B}{C}} = \sqrt{\frac{Z}{Y\left(2+ZY\right)}} = Z_c, \tag{1.40a}$$

$$Z_{STL,T} = \sqrt{\frac{B}{C}} = \sqrt{\frac{Z\left(2+ZY\right)}{Y}} = Z_c, \tag{1.40b}$$

$$\theta_{STL} = \cos^{-1}\left(1+ZY\right) = \theta_c. \tag{1.41}$$

At the targeted frequency, Z_{STL} and θ_{STL} are the equivalent characteristic impedance and electrical length of the three-element network as a non-periodic synthesized transmission line. Note that they are a function of frequency and might be equivalent to a uniform transmission line only on a narrowband basis. Similar analysis can be applied to develop a non-periodic synthesized transmission line with an arbitrary network topology, as long as the network is symmetric in configuration. Readers may find this technique repeatedly throughout the book. Last but not the least, although in general the *ABCD* matrix is the most intuitive and straightforward way to complete the design, the analysis could be started with the *Z* or *Y* matrix, as well.

1.3.3 Extraction of Line Parameters from S-Parameters

The propagation parameters of a synthesized transmission line, without or with periodicity, can also be extracted from its two-port *S*-parameters. To illustrate this, the *ABCD* matrix of a general lossy transmission line is first expressed as,

$$\begin{bmatrix} A & B \\ C & D \end{bmatrix} = \begin{bmatrix} \cosh\gamma l & Z_c \sinh\gamma l \\ Y_c \sinh\gamma l & \cosh\gamma l \end{bmatrix}. \tag{1.42}$$

l is the physical length of the line. The relationships between the *ABCD* and *S* matrices are known as

$$A = \left(1+S_{11}-S_{22}-\Delta S\right)/\left(2S_{21}\right) \tag{1.43a}$$

$$B = \left(1+S_{11}+S_{22}+\Delta S\right)Z_o/\left(2S_{21}\right) \tag{1.43b}$$

$$C = \left(1-S_{11}-S_{22}+\Delta S\right)/\left(2S_{21}Z_o\right) \tag{1.43c}$$

$$D = \left(1-S_{11}+S_{22}-\Delta S\right)/\left(2S_{21}\right) \tag{1.43d}$$

where $\Delta S = S_{11}S_{22} - S_{21}S_{12}$ and Z_0 is the system reference impedance.

Given the fact that the lossy transmission line is symmetric and reciprocal, the complex characteristic impedance (Z_c) and propagation constant (γ_g) are, after some manipulation, extracted from (1.42) and (1.43) as [18]:

$$e^{\gamma_g l} = \frac{1 - S_{11}^2 + S_{21}^2 + \sqrt{\left(1 + S_{11}^2 - S_{21}^2\right)^2 - \left(2S_{11}\right)^2}}{2S_{21}}, \tag{1.44}$$

$$Z_c = Z_o \sqrt{\frac{\left(1 + S_{11}\right)^2 - S_{21}^2}{\left(1 - S_{11}\right)^2 - S_{21}^2}}. \tag{1.45}$$

For a synthesized transmission line, the characteristic impedance and propagation constant can be characterized without much effort by using (1.44) and (1.45) as long as its two-port *S*-parameters are specified by simulation or measurement in advance. The procedure has been widely applied to verify the performance of a synthesized line after the synthesis or integration process.

1.4 Lumped and Quasi-Lumped Approaches

In this and the following sections, classical design approaches are introduced successively to show how a synthesized transmission line can be realized and analyzed. Since the 3-dB branch-line coupler, or the quadrature hybrid, is one of the most common building blocks in microwave systems, it will be adopted as the design example in the following sections for comparison. For each design approach, a branch-line coupler realized by ideal components is first simulated, followed by a real example reported in the literature. The readers may compare the responses of the couplers to learn more about the tradeoff in developing a synthesized transmission line with given specifications.

1.4.1 Lumped Networks

Lumped networks are unambiguously the most intuitive way to fulfill non-periodic synthesized transmission lines [19–21]. Figure 1.6 illustrates a typical synthesized line implemented by lumped elements. It is a π-network comprising two shunt capacitors and a series inductor. By using the technique in Sec. 1.3.2, the *ABCD* matrix of the π-network is

$$\begin{bmatrix} 1 & 0 \\ j\omega C & 1 \end{bmatrix} \begin{bmatrix} 1 & j\omega L \\ 0 & 1 \end{bmatrix} \begin{bmatrix} 1 & 0 \\ j\omega C & 1 \end{bmatrix} = \begin{bmatrix} 1 - \omega^2 LC & j\omega L \\ j\omega C\left(2 - \omega^2 LC\right) & 1 - \omega^2 LC \end{bmatrix}. \tag{1.46}$$

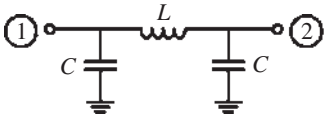

Figure 1.6 Non-periodic synthesized transmission line using a lumped π-network

Meanwhile, the *ABCD* matrix of a lossless uniform transmission line (Z_c, θ) is

$$\begin{bmatrix} A & B \\ C & D \end{bmatrix} = \begin{bmatrix} \cos\theta & jZ_c \sin\theta \\ jY_c \sin\theta & \cos\theta \end{bmatrix}. \tag{1.47}$$

By equating the *ABCD* matrices of the two, the design equations are simplified to

$$\cos\theta = 1 - \omega^2 LC \tag{1.48}$$

$$jZ_c \sin\theta = j\omega L. \tag{1.49}$$

Specifically, the required inductance and capacitance values for a quarter-wavelength synthesized line, with $\theta = \pi/2$, are

$$L = \frac{Z_c}{\omega} \tag{1.50}$$

$$C = \frac{1}{\omega^2 L}. \tag{1.51}$$

An important observation of this sort of synthesized transmission lines is that, unlike a uniform TEM line, the lumped network is lowpass in nature with a cutoff frequency. The 3-dB cutoff frequency can be estimated by

$$f_{cutoff} = \frac{2}{2\pi\sqrt{LC}}. \tag{1.52}$$

In a real design, to preserve phase linearity and non-dispersive characteristic impedance, one should keep in mind that the cutoff frequency of the network should be allocated far away from the targeted operating band to avoid undesired performance degradation.

Using (1.50)–(1.51), the design parameters of a lumped 3-dB quadrature hybrid are summarized in Table 1.2. The center operating frequency for demonstration is set as 1 GHz. The circuit topology is shown in Fig. 1.7(a). The quadrature hybrid consists of pairs of 50- and 35-Ω quarter-wavelength synthesized transmission lines. The simulated *S*-parameters and phase difference between coupled and thru ports are illustrated in Fig. 1.8. The response is somewhat asymmetric with respect to the center frequency, a result of the dispersive nature of the line equivalence. In general, the coupler developed by using the lumped approach has a

Table 1.2 Design parameters of a 1-GHz lumped branch-line coupler

Z_c(Ω)	Frequency (GHz)	$L_{1,2}$ (nH)	$C_{1,2}$ (pF)
50	1	7.958	3.183
35.4	1	5.626	4.502

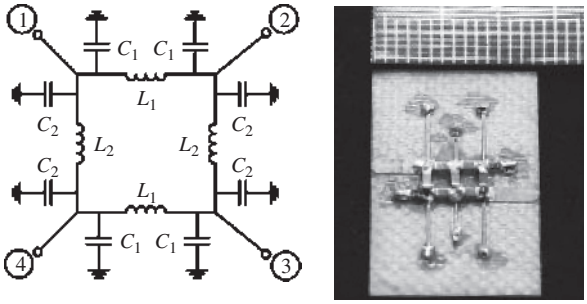

Figure 1.7 Lumped 3-dB branch-line coupler: (a) circuit topology and (b) a design example. Source: Chiang 2001 [22]. Reproduced with permission of IEEE

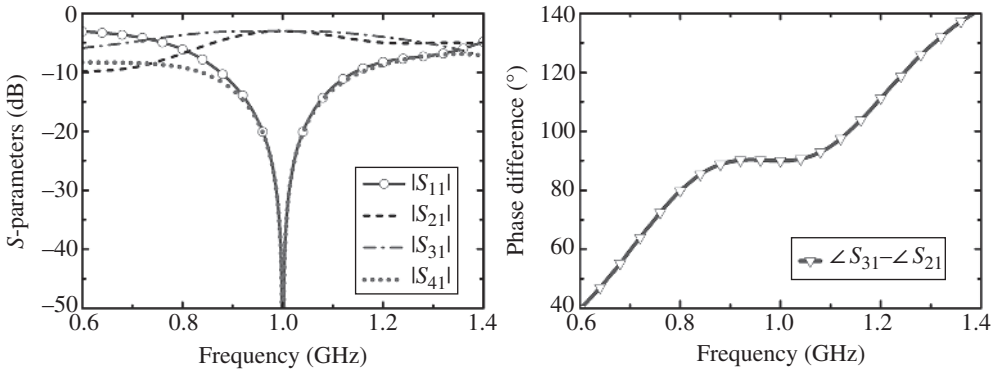

Figure 1.8 *S*-parameters and phase difference of the lumped coupler

narrower bandwidth than its conventional counterpart. The reduced operating bandwidth can be attributed to the fact that the synthesis equations (1.50)–(1.51) are exact only at the center frequency. Figure 1.7(b) shows the layout of an alternative design [22]. It is realized by lumped π-networks composed of series capacitors and shunt inductors. The alternative network is high-pass or left-handed in nature, but the formulation and line equivalence are the same. Readers may refer to Sec. 1.7 for more information on the circuit realization of metamaterials.

Commercial SMD (surface-mounted device) components are frequently used to fulfill lumped couplers on the printed circuit board (PCB); in the IC implementation, the lumped inductors are generally realized on the thick metal layers in meander or spiral shape. The capacitors, in the meantime, can be implemented by metal-oxide-metal (MOM) or metal-insulator-metal (MIM) structures. Ideally, synthesized transmission lines based on the lumped approach could achieve a very high slow wave factor and hence promising miniaturization capability. Nevertheless, in reality, the parasitic loss, or the Q-factor, ultimately sets an upper bound of the achievable size reduction ratio of the design. In addition, the design flexibility may be limited since the off-the-shelf component values may be restricted.

1.4.2 Shunt-Stub Loaded Lines

In addition to the lumped approach, the shunt-stub loaded synthesized transmission lines have received considerable attention [15, 23], as well. A uniform quarter-wavelength line and its open-stub loaded equivalence using the T-model are shown in Fig. 1.9. Following the same procedure in Sec. 1.3.2, the *ABCD* matrix of the quarter-wavelength synthesized line should be identical to that of the uniform one as

$$\begin{bmatrix} \cos\theta_1 & jZ_1\sin\theta_1 \\ jY_1\sin\theta_1 & \cos\theta_1 \end{bmatrix}\begin{bmatrix} 1 & 0 \\ jY_2\tan\theta_2 & 1 \end{bmatrix}\begin{bmatrix} \cos\theta_1 & jZ_1\sin\theta_1 \\ jY_1\sin\theta_1 & \cos\theta_1 \end{bmatrix} = \begin{bmatrix} 0 & jZ_c \\ jY_c & 0 \end{bmatrix}. \quad (1.53)$$

By equating the entries in the matrices, the synthesis equations for a shunt-stub loaded synthesized line can be derived from (1.53) and summarized as

$$Z_1 = \frac{Z_c}{\tan\theta_1} \quad (1.54)$$

$$Y_2\tan\theta_2 = \frac{2}{Z_1\tan 2\theta_1}. \quad (1.55)$$

Since there are only two equations but four unknowns (Z_1, Z_2, θ_1, θ_2), the designer has two degrees of freedom. A variety of circuit layouts, by selecting different variables as the initial parameters, are therefore reported in the literature.

The duality of the T-model, i.e. the π-model in Fig. 1.10, can be equivalent to a quarter-wavelength uniform transmission line, as well. Following the same analysis, the design equations are summarized as

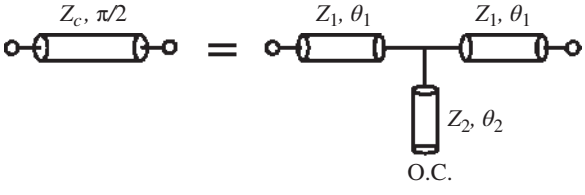

Figure 1.9 A uniform quarter-wavelength line and its equivalent shunt-stub loaded synthesized line using the T-model

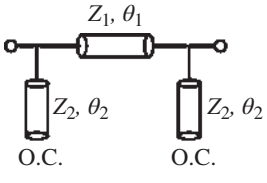

Figure 1.10 A shunt-stub loaded synthesized line based on the π-model

$$Z_1 = \frac{Z_c}{\sin\theta_1} \tag{1.56}$$

$$Y_2 \tan\theta_2 = \frac{\cos\theta_1}{Z_c}. \tag{1.57}$$

A 3-dB branch-line coupler is designed as an example. The operating frequency is also 1 GHz for easy comparison. The T-model in Fig. 1.9 is adopted as the building block. Let $\theta_1 = 30^o$ and $Z_2 = 30\ \Omega$ for the 35- and 50-Ω synthesized lines, one can use (1.54)–(1.55) to calculate the remaining parameters as listed in Table 1.3. Figure 1.11 illustrates the *S*-parameters of the coupler; the phase difference between the thru and coupled ports is shown at the same time. The *S*-parameters are asymmetric with respect to the center frequency since the cutoff frequency of the non-periodic synthesized line, also low-pass in nature, may be too close to the band of concern. In addition, the network equivalence in (1.54) and (1.55) is on a narrow-band basis, which may account for the discrepancy, as well.

For efficient usage of the circuit area, the open stub in the synthesized line can be further split into multiple stubs. Figure 1.12 shows an example by replacing the original stub with two open stubs connected in parallel [23]. The design equation is straightforward as

$$\frac{Z_a \tan\theta - Z_c \tan\theta_a}{Z_a^2 \tan\theta \tan\theta_a + Z_c Z_a} = Y_1 \tan\theta_1 + Y_2 \tan\theta_2. \tag{1.58}$$

Table 1.3 Design parameters of a 1-GHz shunt-stub branch-line coupler

Z_c (Ω)	Frequency (GHz)	Z_1 (Ω)	θ_1(°)	Z_2 (Ω)	θ_2(°)
50	1	86.60	30	30	21.8
35.4	1	61.23	30	30	29.5

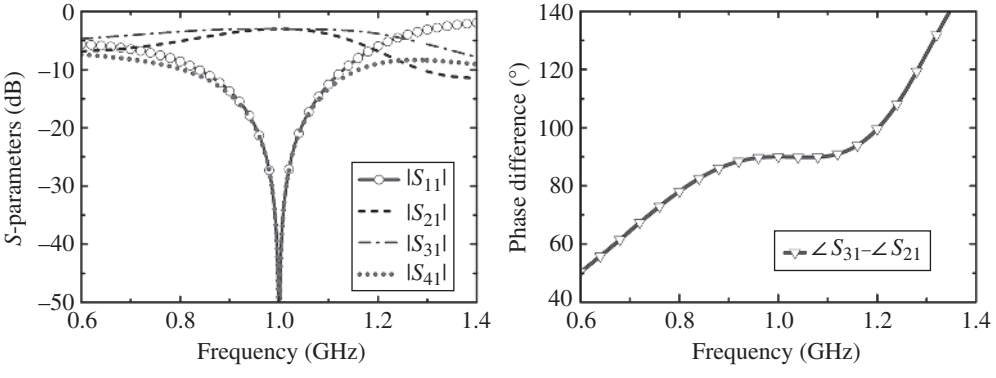

Figure 1.11 *S*-parameters and phase difference of the 3-dB coupler realized by loaded shunt stubs

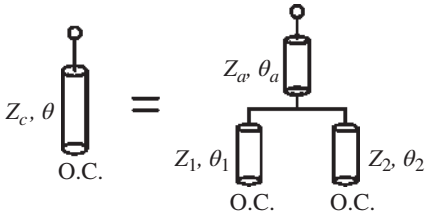

Figure 1.12 Splitting a single stub into dual open stubs in parallel connection

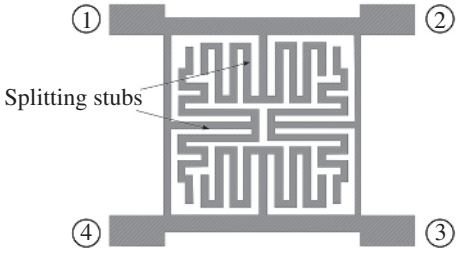

Figure 1.13 Typical layout of a shunt-stub loaded coupler using split open stubs. Source: Tang 2007 [23]. Reproduced with permission of IEEE

Figure 1.13 shows the typical layout of a 3-dB quadrature hybrid using split stubs. The stubs are meandered to fill out the inner space of the coupler. It is 23.5% the size of a conventional design. Splitting a single stub into triple or even more stubs for circuit miniaturization is also possible, yet the parasitic coupling between adjacent lines makes the design highly dependent on an EM simulator to optimize the layout for good responses.

The ways to implement synthesized transmission lines using non-periodic lumped/quasi-lumped networks are included but not limited to the aforementioned approaches. For example, the bridged T-coil in [24] is a very elegant way to fulfill a very compact design. The readers can find more design examples and new ideas in Chapter 2 about PCB designs and in Chapter 5 about on-chip realization.

1.5 One-Dimensional Periodic Structures

Periodic structures are also a popular way to realize synthesized transmission lines for circuit miniaturization [25, 26]. In this section, one-dimensional periodic structures will be analyzed using the Bloch wave analysis in Sec. 1.3.1; the two-dimensional ones, in the meantime, will be covered in Sec. 1.6.

In general, a one-dimensional periodic synthesized line is composed of periodically-loaded inductors and capacitors, and can be directly mapped to the distributed transmission-line model in Fig. 1.2. Figure 1.14(a) shows a typical one-dimensional periodic synthesized line. The unit cell can be represented by either a T- or π-model. As an example, the T-model is discussed in terms of the two-port z-parameters in Fig. 1.14(b). According to (1.30) and Fig. 1.14(b), the propagation constant can be expressed as

$$\cosh(\gamma p) = \frac{A+D}{2} = \frac{Z_{11}+Z_{22}}{2Z_{12}}. \tag{1.59}$$

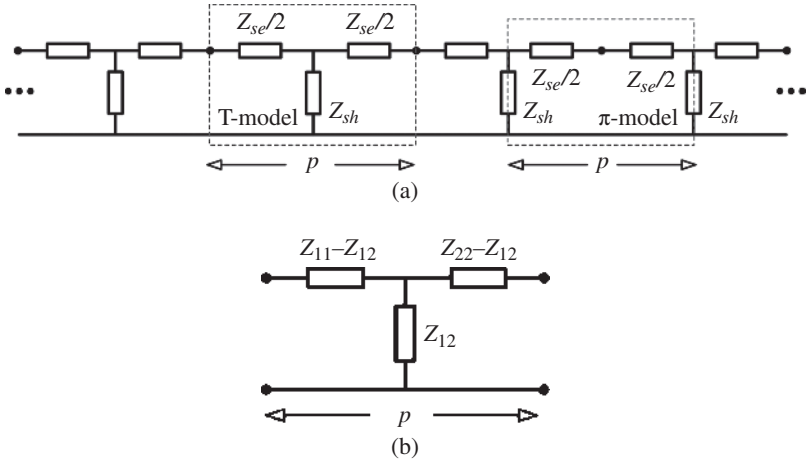

Figure 1.14 Typical one-dimensional periodic synthesized transmission line: (a) infinite unit cells in cascade and (b) two-port *Z*-parameters of the unit cell using the T-model

Since the unit cell is much smaller than the guided wavelength ($p << \lambda_g$), the hyper-trigonometric function can be simplified to:

$$\cosh(\gamma p) \cong 1 + \frac{(\gamma p)^2}{2}. \tag{1.60}$$

Substitution of (1.60) into (1.59) gets,

$$(\gamma p)^2 = \frac{Z_{11} + Z_{22} - 2Z_{12}}{Z_{12}} \equiv \frac{Z_{se}}{Z_{sh}}. \tag{1.61}$$

Here, Z_{se} is the direct sum of the series impedances of the T-network, and Z_{sh} is the impedance of the shunt stub. The propagation constant is therefore characterized by

$$\gamma = \alpha + j\beta = \frac{1}{p}\sqrt{\frac{Z_{se}}{Z_{sh}}}, \tag{1.62}$$

and the Bloch impedance of the periodic synthesized line is

$$Z_B = \sqrt{Z_{se} Z_{sh}}. \tag{1.63}$$

Equations (1.62)–(1.63) are the design basis of a one-dimensional periodic synthesized transmission line.

Consider again the 1-GHz branch-line coupler. Based on the T-model, a lossless periodic *LC* network is shown in Fig. 1.15. The series impedance (Z_{se}) and shunt impedance (Z_{sh}) are, respectively,

$$Z_{se} = j\omega L \tag{1.64a}$$

$$Z_{sh} = 1/\, j\omega C. \tag{1.64b}$$

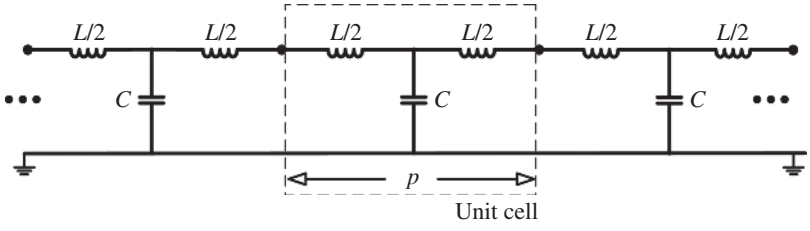

Figure 1.15 A periodic synthesized transmission line using T-model unit cells

Table 1.4 Parameters of a 3-dB branch-line coupler by periodic lumped *LC* unit cells

$Z_c(\Omega)$	Frequency (GHz)	N_{UC}	C (pF)	L (nH)
50	1	30	0.1667	0.4167
35.4	1	25	0.2829	0.3535

Substitution of (1.64) into (1.62) and (1.63) yields,

$$j\beta = \frac{1}{p} \cdot j\omega\sqrt{LC} \tag{1.65}$$

$$Z_c = \sqrt{\frac{L}{C}}. \tag{1.66}$$

If the number of unit cells in a quarter-wavelength line is specified as N_{UC}, the design equations for the inductance and capacitance values in each unit cell become

$$C = \frac{\pi/2}{N_{UC}}\left(\frac{1}{\omega Z_c}\right) \tag{1.67}$$

$$L = Z_c^2 \cdot C. \tag{1.68}$$

Using (1.67) and (1.68), the parameters for realizing a 1-GHz branch-line coupler are summarized in Table 1.4. The numbers of unit cells in the 35-Ω and 50-Ω periodic synthesized lines are 25 and 30, respectively. Figure 1.16 shows its corresponding *S*-parameters and phase difference. Since the periodic structure is more similar in topology to a uniform transmission line, the operating bandwidth of the coupler is very similar to that of a conventional design. The cutoff frequency of the synthesized line also reflects the same trend. For this specific design, the cut-off frequency of the unit cell is as high as 18.9 GHz, making the responses very symmetric with respect to the center frequency.

In a real design, the inductors and capacitors in the one-dimensional periodic structure are commonly realized by high-impedance lines and shunt open stubs, respectively. Although the design methodology is similar, one should be aware that since there are only two requisite

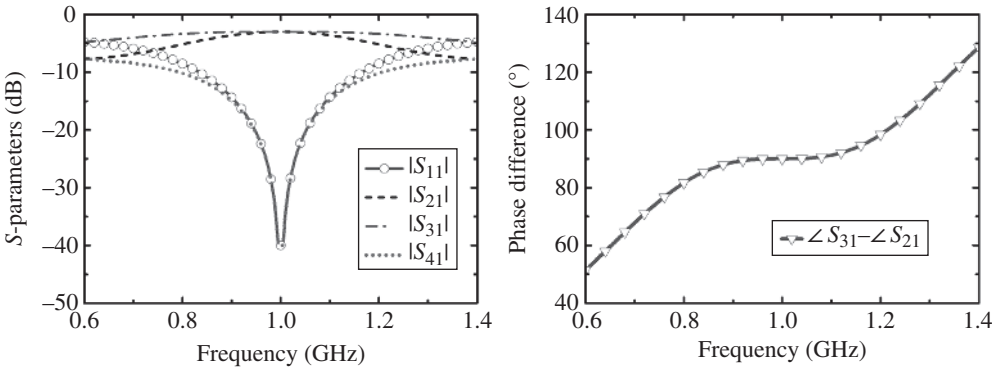

Figure 1.16 *S*-parameters and phase difference of the 3-dB coupler by one-dimensional periodic synthesized lines with lumped *LC* sections

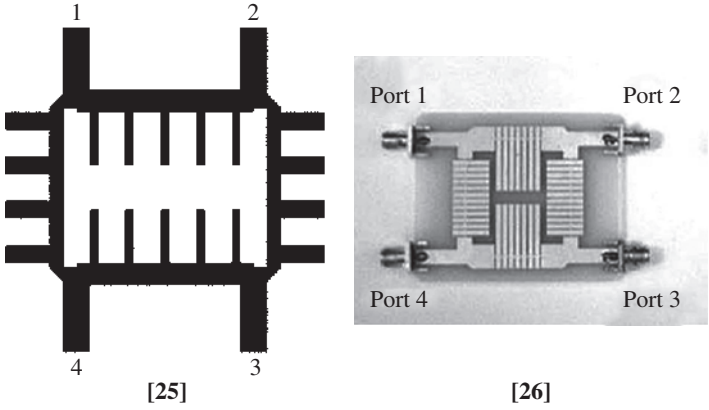

[25] **[26]**

Figure 1.17 Design examples of quadrature hybrids using periodic synthesized transmission lines. Source: Eccleston 2003 [25]; Sun 2005 [26]. Reproduced with permission of IEEE

conditions (Z_c, θ) but four unknowns (characteristic impedances and electrical lengths of the series/shunt lines), a number of topologies with equal electrical properties can be developed for layout optimization and circuit miniaturization. Typical examples are shown in Fig. 1.17. The number of unit cells in a quarter-wavelength line varies from 4 to 12. Readers may also use the same procedure to develop their own periodic synthesized transmission lines with a unique layout arrangement.

1.5.1 Complementary-Conducting-Strip Lines

The complementary-conducting-strip (CCS) line is a one-dimensional periodic synthesized line especially suitable for semiconductor fabrication processes. It can facilitate two-dimensional routing and has been widely used in microwave systems [2, 3, 27–29]. Figure 1.18(a) shows the unit cell of a typical CCS transmission line. The signal trace is composed of a central patch

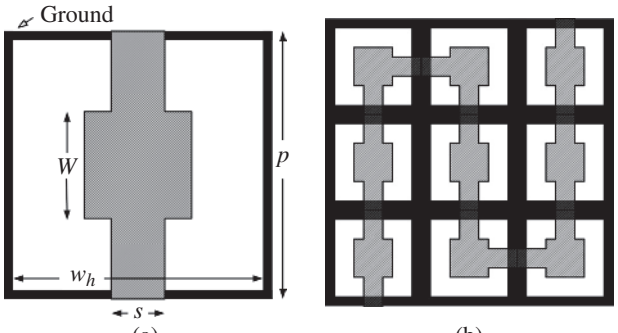

Figure 1.18 CCS synthesized transmission line: (a) unit cell and (b) a meander line

and connection arms. The widths of the patch and connection arm are w and s, respectively. The ground plane is deposited around the patch with a mesh area of $w_h \times w_h$. Since the arms of the CCS cell can be connected to two out of four directions, the CCS line can fulfill two-dimensional routing with very efficient usage of the circuit area for miniaturization.

The Bloch wave analysis in Sec. 1.3.1 can be again applied to develop the line. The periodicity of the unit cell, which should be much smaller than the guided wavelength, is denoted as p. The shunt capacitance is determined by the overlapped area between the ground plane mesh ($w_h \times w_h$) and signal trace (s). Increasing the overlapped area raises the capacitance. The inductance is determined by the patch width (w) as well as the signal trace (s). Since the inductance and capacitance of a CCS cell can be determined independently, one can fulfill a two-dimensional routing with a wide variety of characteristic impedances.

A design example is discussed for clear illustration. In a 1P6M 0.18 μm CMOS process, the design parameters for a CCS unit cell are $p = 30$ μm, $w_h = 29$ μm, $w = 5$ μm, and $s = 3$ μm [29]. The thicknesses of the signal trace and meshed ground plane are 2.39 and 6.05 μm, respectively. By a cascade connection of nine unit cells, the layout of the meander line is shown in Fig. 1.18(b); the total length is 270 μm. By using an EM simulator, the S-parameters of the CCS sample at 24 GHz are $S_{11} = 0.053 + j0.088$ and $S_{21} = 0.921 - j0.304$. The extracted characteristic impedance from (1.45) is $70.28 - j3.59\ \Omega$. The image part accounts for the conductor and dielectric losses. The slow-wave factor and quality factor at 24 GHz are 2.25 and 7.6, respectively.

The CCS synthesized line is non-dispersive over a wide frequency range. As a rule of thumb, the variation of the characteristic impedance of the meander line in Fig. 1.18(b) is less than 3.6% from 10 to 40 GHz. Its slow wave factor, which is around 2.3, is actually not remarkable at all. Nevertheless, the two-dimensional routing capability makes the CCS line become a promising solution for circuit miniaturization with great layout flexibility.

1.6 Photonic Bandgap Structures

The photonic bandgap (PBG) structure is a real two-dimensional synthesized transmission line. Unlike the previous cases, the periodic patterns are fabricated on the entire ground plane rather than the signal trace [30, 31]. Figure 1.19 illustrates the typical layout of nine PBG unit cells. Each unit cell consists of a square metal pad along with four connecting arms. The ground

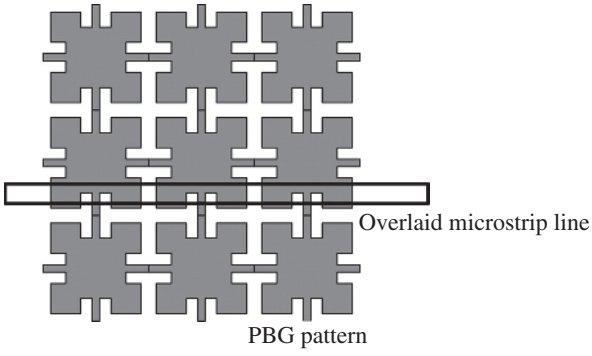

Figure 1.19 A typical PBG structure with an overlaid microstrip line

plane is etched with a periodic pattern, and the signal trace above the ground plane could be any sort of conventional transmission line, such as a microstrip line. While the narrow arms of the unit cell lead to additional inductance, the coupling between nearby pads raises the overall capacitance. The structure hence reveals slow-wave characteristics.

Despite its slow-wave nature, the main purpose of PBG structures is to introduce bandgap phenomenon for mode suppression, system isolation, and so on. During the design phase, a full-wave EM simulator is always required to complete the design since analyzing the PBG structure using simple circuit models is nearly impossible. For interested readers, more information can be found in [30].

1.7 Left-Handed Structures

Left-handed structures, or the metamaterials, are also a popular solution not only for size miniaturization but also for realizing a number of circuits not feasible by conventional righted-handed components. For example, dual-band designs with a non-integer ratio between passbands, beam-switching agility of leaky-wave antennas, and so on are realized and demonstrated [32, 33]. In fact, the concept of metamaterials is not new, and can be traced back to 1967 by a Russian physicist, Victor Veselago [34]. Nevertheless, it was not introduced to the microwave and antenna communities until the late 1990s and early 2000s. After the induction, related research was boosted dramatically, and this has been recognized as one of the main streams in the 2010s. The interested readers may found more information in a number of books such as [35, 36].

As shown in Fig. 1.20(a), a pure left-handed transmission line is a periodic structure consisting of alternatively connected series capacitance and shunt inductance. By using the Bloch wave analysis in Sec. 1.3.1, the propagation characteristics of the left-handed structure can be extracted. Some interesting phenomena, such as negative permittivity and permeability, anti-parallel phase and group velocities, and so on are observed. However in the real implementation, since the series capacitance and shunt inductance are inevitably connected to one another by conventional, or right-handed, transmission lines, a more realistic model named the composite right/left-handed (CRLH) transmission line was proposed and analyzed. Referring to Fig. 1.20(b), the CRLH line consists of periodically connected series *LC* resonator in the serial path and parallel *LC* resonator in the shunt path. While the C_L and L_L are the left-handed components, the C_R and L_R account for the right-handed connecting lines.

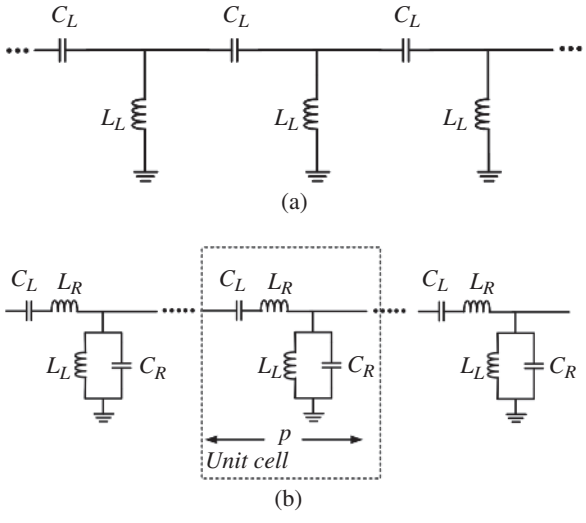

Figure 1.20 Periodic unit cells of (a) a pure left-handed synthesized line and (b) a composite right/left handed (CRLH) transmission line

The propagation constant and characteristic impedance, under a lossless assumption, can be solved from (1.62) and (1.63) as

$$\beta = \frac{1}{p}\cos^{-1}\left[1-\frac{1}{2}\left(\frac{\omega_L^2}{\omega^2}+\frac{\omega^2}{\omega_R^2}-\frac{\omega_L^2}{\omega_{se}^2}-\frac{\omega_L^2}{\omega_{sh}^2}\right)\right] \tag{1.69}$$

$$Z_c = \sqrt{\frac{L_L}{C_L}}\cdot\sqrt{\frac{\omega^2/\omega_{se}^2-1}{\omega^2/\omega_{sh}^2-1}} \tag{1.70}$$

where

$$\omega_L = \frac{1}{\sqrt{C_L L_L}} \quad \omega_R = \frac{1}{\sqrt{C_R L_R}} \quad \omega_{se} = \frac{1}{\sqrt{C_L L_R}} \quad \omega_{sh} = \frac{1}{\sqrt{C_R L_L}}. \tag{1.71}$$

p is the periodicity. If one further assumes

$$\omega_{se} = \frac{1}{\sqrt{C_L L_R}} = \frac{1}{\sqrt{C_R L_L}} = \omega_{sh}, \tag{1.72}$$

the CRLH line is said to be balanced so that the equations are reduced as

$$\beta = \omega\sqrt{L_R C_R} - \frac{1}{\omega\sqrt{L_L C_L}} \tag{1.73}$$

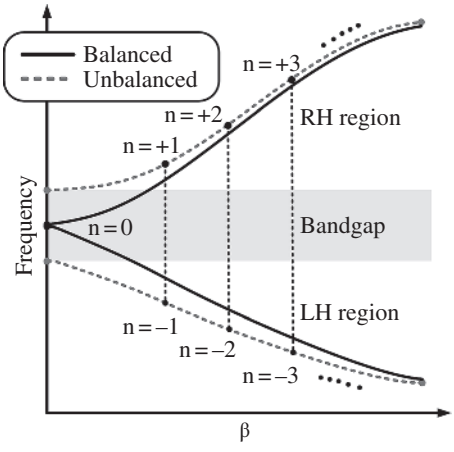

Figure 1.21 Dispersion diagrams of the balanced and unbalanced CRLH lines

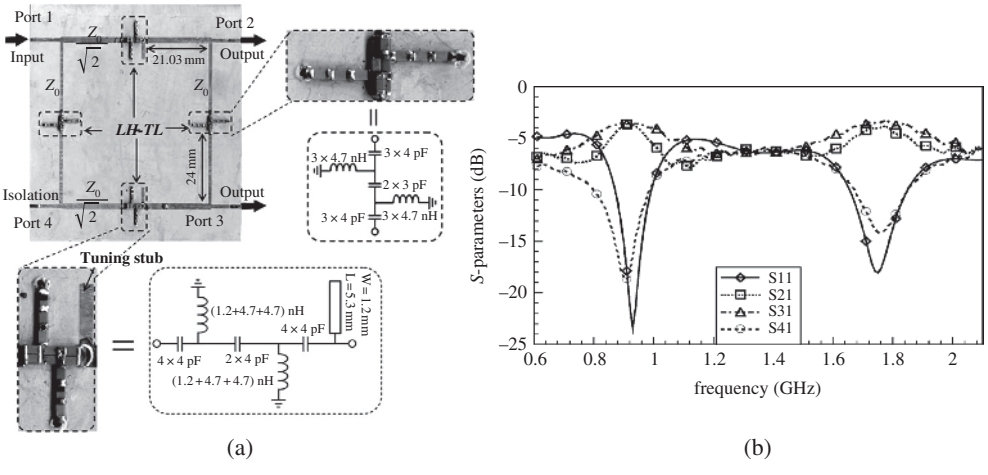

Figure 1.22 (a) Layout and (b) *S*-parameters (measurement) of a dual-band branch-line coupler using CRLH lines. Source: Lin 2004 [37]. Reproduced with permission of IEEE

$$Z_c = \sqrt{\frac{L_L}{C_L}} = \sqrt{\frac{L_R}{C_R}}. \tag{1.74}$$

Figure 1.21 compares the dispersion diagrams of the balanced and unbalanced CRLH transmission lines. For the unbalanced case, a bandgap between the left-handed and right-handed passbands is clearly observed. With the balanced condition, the bandgap is disappeared and the operating band becomes continuous. A number of positive as well as negative resonance modes, occurring when $\beta p = \pm n\pi$, are observed. They have been widely applied to various applications with distinct circuit properties.

Figure 1.22(a) shows a typical design example, which is a dual-band branch-line coupler [37]. Each CRLH line is realized by a pair of conventional microstrip lines along with two

T-model left-handed unit cells. The ratio between the operating frequency bands, as shown in Fig. 1.22(b), is a non-integer. This feature is not attainable by uniform wave-guiding structures. A left-handed synthesized line without periodicity is also realizable. In this case, the network could be analyzed using the *ABCD* matrix as mentioned in Sec. 1.3.2. Generally, it comprises a number of series capacitors and shunt inductors in cascade and is highpass in nature. A number of left-handed synthesized lines are developed in the following chapters to utilize their unusual frequency responses to fulfill design goals such as multi-mode operation.

References

[1] C. Z. Li and J. S. Lin, *Microwave Noncontact Motion Sensing and Analysis*, 1st edn, John Wiley & Sons, Ltd, Chichester, UK, 2013.

[2] S. Wang, K.-H. Tsai, K.-K. Huang, and M.-S. Kang, S.-X. Li, H.-S. Wu and C.-K. C. Tzuang, "Design of *X*-band RF CMOS transceiver for FMCW monopulse radar," *IEEE Trans. Microw. Theory Techn.*, vol. 57, no. 1, pp. 61–70, Jan. 2009.

[3] H.-S. Wu, C.-W. Wang, and C.-K. C. Tzuang, "CMOS active quasi-circulator with dual transmission gains incorporating feedforward technique at *K*-band," *IEEE Trans. Microw. Theory Techn.*, vol. 58, no. 8, pp. 2084–2091, Aug. 2010.

[4] P. Pursula, T. Karttaavi, M. Kantanen, A. Lamminen, J. Holmberg, M. Lahdes, et al., "60-GHz millimeter-wave identification reader on 90-nm CMOS and LTCC," *IEEE Trans. Microw. Theory Techn.*, vol. 59, no. 4, pp. 1166–1173, Apr. 2011.

[5] J.-L. Kuo, Y.-F. Lu, T.-Y. Huang, Y.-L. Chang, Y.-K. Hsieh, P.-J. Peng, et al., "60-GHz four-element phased-array transmit/receive system-in-package using phase compensation techniques in 65-nm flip-chip CMOS process," *IEEE Trans. Microw. Theory Techn.*, vol. 60, no. 3, pp. 743–756, Mar. 2012.

[6] S.-Y. Kim, O. Inac, C.-Y. Kim, D. Shin, and G. M. Rebeiz, "A 76–84-GHz 16-element phased-array receiver with a chip-level built-in self-test system," *IEEE Trans. Microw. Theory Techn.*, vol. 61, no. 8, pp. 3083–3098, Aug. 2013.

[7] P. Kurgan, J. Filipcewicz, and M. Kitlinski, "Development of a compact microstrip resonant cell aimed at efficient microwave component size reduction," *IET Microwaves, Antennas & Propagation.*, vol. 6, no. 12, pp. 1291–1298, Aug. 2012.

[8] J.-S. Hong and M. J. Lancaster, "Theory and experiment of novel microstrip slow-wave open-loop resonator filters," *IEEE Trans. Microw. Theory Techn.*, vol. 45, no. 12, pp. 2358–2365, Dec. 1997.

[9] C. Karpuz, "Bandstop characteristics of a triangular microstrip slotted patch as an electromagnetic bandgap (EBG)," *Microw. Opt. Technol. Lett.*, vol. 36, no. 3, pp. 149–150, Jan. 2003.

[10] G. Cakir and L. Sevgi, "A design of novel microstrip electromagnetic bandgap (EBG) structure," *Microw. Opt. Technol. Lett.*, vol. 46, no.4, pp. 399–401, Jun. 2005.

[11] M. Hayati and A. Lotfi, "Compact lowpass filter with high and wide rejection in stopband using front coupled tapered CMRC," *Electron. Lett.*, vol. 46, no.12, pp. 846–848, Jun. 2010.

[12] K.W. Eccleston and S.H.M. Ong, "Compact planar microstripline branch-line and rat-race couplers," *IEEE Trans. Microw. Theory Techn.*, vol. 51, no. 10, pp. 2119–2125, Oct. 2003.

[13] J. Wang, B. Z. Wang, Y. X. Guo, L. C. Ong, and S. Xiao, "A compact slow-wave microstrip branch-line coupler with high performance," *IEEE Microw. Wireless Compon. Lett.*, vol. 17, no. 7, pp. 501–503, Jul. 2007.

[14] K. S. Chin, K. M. Lin, Y. H. Wei, T. H. Tseng, and Y. J. Yang, "Compact dual-band branch-line and rat-race couplers with stepped-impedance-stub lines," *IEEE Trans. Microw. Theory Techn.*, vol. 58, no. 5, pp. 1213–1221, May. 2010.

[15] C. H. Tseng and H. J. Chen, "Compact rat-race coupler using shunt-stub-based artificial transmission lines," *IEEE Microw. Wireless. Compon. Lett.*, vol. 18, no. 11, pp. 734–736, Nov. 2008.

[16] J. He, B. Z. Wang, and W. Shao, "Compact power divider embedded with zigzag microstrip slow-wave structures," *Electron. Lett.*, vol. 45, no. 1, pp. 62–63, Jan. 2009.

[17] R. E. Collin, *Foundations for Microwave Engineering*, 2nd edn, New York: McGraw-Hill, 1992.

[18] W.-R. Eisenstadt and Y. Eo, "S-parameter-based IC interconnect transmission line characterization," *IEEE Trans. Comp., Hybrids, Manufact. Technol.*, vol. 15, pp. 483–490, Aug. 1992.

[19] R.-W. Vogel, "Analysis and design of lumped- and lumped-distributed-element directional couplers for MIC and MMIC applications," *IEEE Trans. Microw. Theory Techn.*, vol. 40, no. 2, pp. 253–262, Feb. 1992.
[20] E. Gandini, M. Ettorre, R. Sauleau, and A. Grbic, "A lumped-element unit cell for beam-forming networks and its application to a miniaturized Butler matrix," *IEEE Trans. Microw. Theory Techn.*, vol. 61, no. 4, pp. 1477–1487, Apr. 2013.
[21] B. Cetinoneri, Y.-A. Atesal, and G. M. Rebeiz, "An 8×8 Butler matrix in 0.13-μm CMOS for 5–6-GHz multi-beam applications," *IEEE Trans. Microw. Theory Techn.*, vol. 59, no. 2, pp. 295–301, Feb. 2011.
[22] Y.-C. Chiang and C.-Y. Chen, "Design of a wide-band lumped-element 3-dB quadrature coupler," *IEEE Trans. Microwave Theory Techn.*, vol. 49, no. 3, pp. 476–479, Mar. 2001.
[23] C.-W. Tang and M.-G. Chen, "Synthesizing microstrip branch-line couplers with predetermined compact size and bandwidth," *IEEE Trans. Microw. Theory Techn.*, vol. 55, no. 9, pp. 1926–1934, Sept. 2007.
[24] Y.-S. Lin and J.-H. Lee, "Miniature Butler matrix design using glass-based thin-film integrated passive device technology for 2.5-GHz applications," *IEEE Trans. Microw. Theory Techn.*, vol. 61, no. 7, pp. 2594–2602, July 2013.
[25] K.-W. Eccleston and S.-H. M. Ong, "Compact planar microstripline branch-Line and rat-race couplers," *IEEE Trans. Microw. Theory Techn.*, vol. 51, no. 10, pp. 2119–2125, Oct. 2003.
[26] K.-O. Sun, S.-J. Ho, C.-C. Yen, and D.-Van D. Weide, "A compact branch-line coupler using discontinuous microstrip lines," *IEEE Microw. Wireless Compon. Lett.*, vol. 15, no. 8, pp. 519–520, Aug. 2005.
[27] C.-C. Chen and C.-K. C. Tzuang, "Synthesized quasi-TEM meandered transmission lines for compacted microwave integrated circuits," *IEEE Trans. Microw. Theory Techn.*, vol. 52, no. 6, pp. 1637–1647, Jun. 2004.
[28] M.-J. Chiang, H.-S. Wu, and C.-K. C. Tzuang, "Design of synthesized quasi-TEM transmission line for CMOS compact integrated circuit," *IEEE Trans. Microw. Theory Techn.*, vol. 55, no. 12, pp. 2512–2520, Dec. 2007.
[29] C.-W. Wang, H.-S. Wu, and C.-K. C. Tzuang, "CMOS passive phase shifter with group-delay deviation of 6.3 ps at *K*-Band," *IEEE Trans. Microw. Theory Techn.*, vol. 59, no. 7, pp. 1778–1786, Jul. 2011.
[30] F.-R. Yang, K.-P. Ma, Y. Qian, and Tatsuo Itoh, "A uniplanar compact photonic-bandgap (UC-PBG) structure and its applications for microwave circuits," *IEEE Trans. Microw. Theory Techn.*, vol. 47, no. 8, pp. 1509–1514, Aug. 1999.
[31] F.-R. Yang, Y. Qian, R. Coccioli, and T. Itoh, "A novel low-loss slow-wave microstrip structure," *IEEE Microw. Guided Wave Lett.*, vol. 8, no. 11, pp. 372–374, Nov. 1998.
[32] G. V. Eleftheriades, "Enabling RF/microwave devices using negative refractive-index transmission-line (NRI-TL) metamaterials," *IEEE Antennas Propag. Mag.*, vol. 49, no. 2, pp. 34–51, Apr. 2007.
[33] C. Caloz, T. Itoh, and A. Rennings, "CRLH metamaterial leaky-wave and resonant antennas," *IEEE Antennas Propag. Mag.*, vol. 50, no. 5, pp. 25–39, Oct. 2008.
[34] V. G. Veselago, "The electrodynamics of substances with simultaneously negative value of ε and μ," *Soviet Phys. Uspekhi*, vol. 10, no. 4, pp. 509–514, Jan. 1968.
[35] N. Engheta and R. W. Ziolkowski, *Metamaterial: Physics and Engineering Explorations*, 1st edn, John Wiley & Sons, Ltd, Chichester, UK, 2006.
[36] C. Caloz and T. Itoh, *Electromagnetic Metamaterials: Transmission Line Theory and Microwave Applications*, Wiley-IEEE Press, Chichester, UK, 2005.
[37] I.-H. Lin, M. DeVincentis, C. Caloz, and T. Itoh, "Arbitrary dual-band components using composite right/left-handed transmission lines," *IEEE Trans. Microw. Theory Techn.*, vol. 52, no. 4, pp. 1142–1149, Apr. 2004.